Effects of groundwater pumping on ground surface temperature: A regional modeling study in the North China Plain

Chen Yang[1,2,3], Hong-Yi Li[3], Yilin Fang[4], Chixiao Cui[5], Tianye Wang[6,7], Chunmiao Zheng[1,2], L. Ruby Leung[4], Reed M. Maxwell[8], You-Kuan Zhang[1,2*], Xiaofan Yang[9,10*]

[1]Guangdong Provincial Key Laboratory of Soil and Groundwater Pollution Control, School of Environmental Science and Engineering, Southern University of Science and Technology, Shenzhen 518055, China.

[2]State Environmental Protection Key Laboratory of Integrated Surface Water-Groundwater Pollution Control, School of Environmental Science and Engineering, Southern University of Science and Technology, Shenzhen 518055, China.

[3]Cullen College of Engineering, University of Houston, Houston, TX 77204, USA.

[4]Pacific Northwest National Laboratory, Richland, WA 99354, USA.

[5]Taihu Lake Laboratory Ecosystem Research Station, State Key Laboratory of Lake Science and Environment, Nanjing Institute of Geography and Limnology, Chinese Academy of Sciences, Nanjing 21008, China.

[6]Key Laboratory of Water Cycle and Related Land Surface Processes, Institute of Geographic Sciences and Natural Resources Research, Chinese Academy of Sciences, Beijing 100101, China.

[7]University of Chinese Academy of Sciences, Beijing 100049, China.

[8]Department of Geology and Geological Engineering, Colorado School of Mines, Golden, CO 80401, USA.

[9]State Key Laboratory of Earth Surface Processes and Resource Ecology, Faculty of Geographical Science, Beijing Normal University, Beijing 100875, China.

[10]Beijing Computational Science Research Center, Beijing 100195, China.

Corresponding author:
Xiaofan Yang (xfyang@bnu.edu.cn); You-Kuan Zhang (zhangyk@sustech.edu.cn)

Key Points

- Effects of groundwater pumping on ground surface temperature (GST) in the North China Plain is investigated using an integrated model.

- Groundwater pumping increases the annual average ground surface temperature and results in hotter summers and colder winters.

- Effects of groundwater pumping on GST may last for 20 years, with larger effect in the beginning due to nonlinear response.

Abstract

Over-exploitation of groundwater (GW) in the North China Plain (NCP) since the 1960s has many environmental consequences. However, understanding of the dominant mechanisms remains limited, particularly at the regional scale. In this study, the coupled ParFlow.CLM model representing subsurface and land-surface processes and their interactions was applied in the NCP at high spatio-temporal resolutions. The model was validated using the water and energy fluxes reported in previous studies and from the JRA-55 reanalysis. Numerical experiments were designed to examine the relative impacts of GW pumping and irrigation on the ground surface temperature (GST). Results showed significant effects of GW pumping on GST in the NCP. Generally, the subsurface acts as a buffer to temporal variations in heat fluxes at the land-surface, but long-term pumping can gradually weaken this buffer, resulting in increases in the spatio-temporal variability of GST, as exemplified by hotter summers and colder winters. Considering that changes of water table depth (WTD) can significantly affect land surface heat fluxes when WTD ranges roughly between 1–10 m, the 0.5 m/year increase of WTD simulated by the model due to pumping can continue to increase the average WTD and hence, GST, for about 20 years from the pre-pumping WTD in the NCP, before the WTD exceeds 10 m. The increase of GST is expected to be faster initially and gradually slow down due to the nonlinear increase of GST with WTD. The findings from this study in the NCP may also have implications for other regions with GW depletion.

1. Introduction

Ground surface temperature (GST) and soil temperature (ST) have important influence on terristrial processes such as ecosystem functions, surface-subsurface interactions, and land-atmosphere interactions, with implications for how the terrestrial system responds to climate change [*H Zhang et al.*, 2016]. For example, ST controls the growth of vegetation, which is extremely sensitive to temperature, so it is a major factor influencing crop yield in agricultural regions [*H Zhang et al.*, 2016]. The increase in ST has accelerated soil respiration, with a 20% increase in soil respiration corresponding to a release of about 14–20 PgC/yr soil carbon, which is 2–3 times the amount of carbon released from fossil fuel and land use change (7 PgC/yr) [*Davidson et al.*, 2006; *Lloyd and Taylor*, 1994].

GW is an important source of fresh water in many populated regions such as the North China Plain (NCP), which is the political, economic, and agricultural center of China. Over-exploitation of GW in the NCP since the 1960s mainly for irrigation has many environmental consequences, such as river deterioration, land subsidence, and seawater intrusion [*C M Liu et al.*, 2001]. Water table depth (WTD) in most places of the NCP is now more than tens of meters, much deeper than 1–3 m during the 1960s, with some regions such as Beijing, Shijiazhuang, and Cangzhou showing WTD of more than one hundred meters [*Cao et al.*, 2013]. Meanwhile, with climate change [*Kang and Eltahir*, 2018], the annual average air temperature in the NCP has increased by 0.23 °C per decade, which is slightly higher than the global average during the same period [*A et al.*, 2016]. The rising air temperature could lead to the changes in GST [*Pollack et al.*, 2005].

Figure 1 shows the variations of GST and WTD in the NCP for the last 40 years. With increasing trends in both GST and WTD, an important question is whether the GW withdrawal may have contributed to the increasing GST, although the latter has generally been attributed to the increasing air temperature [*Pollack et al.*, 2005; *H Zhang et al.*, 2016; *T Zhang et al.*, 2001]. Recent studies addressing the important role of GW in the subsurface–land-surface–atmosphere system [*Keune et al.*, 2016; *R. M. Maxwell and Condon*, 2016; *Taylor et al.*, 2013] noted the important control of GW on soil moisture that governs the land surface energy fluxes, with subsequent influence on local weather and climate through land-atmosphere interactions [*Ferguson and Maxwell*, 2012]. However, few studies have looked at the impact of human activities such as GW pumping or irrigation on GST at the regional scale. During the rapid socioeconomic development over the NCP in the past few decades, GW pumping has been

91   extensively utilized to overcome shortages in fresh water resources [*Cao et al.*, 2013; *C M Liu et*
92   *al.*, 2001].

93
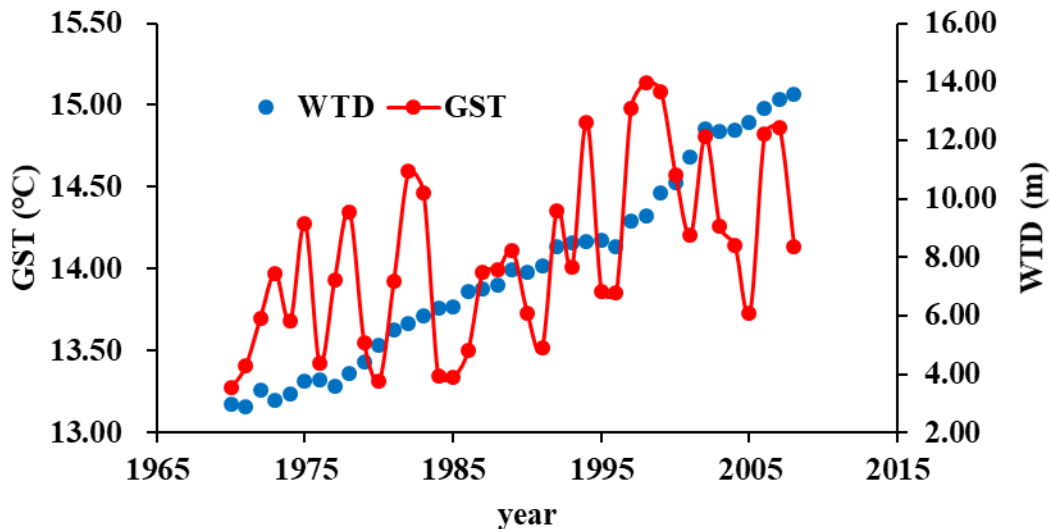
94
95   **Figure 1. Yearly variations in GST and WTD from 1970 to 2008 in the NCP. GST is at the center of**
96   **the NCP from JRA-55 reanalysis data [*Harada et al.*, 2016; *Kobayashi et al.*, 2015]; while WTD is the**
97   **regional average from a previous modeling study [*Cao et al.*, 2013].**

98
99   GW movements and pumping in the NCP has been examined by numerous studies using
100   mostly groundwater models such as MODFLOW [*Cao et al.*, 2013; *Cui et al.*, 2009; *Hu et al.*,
101   2010; *Jia and Liu*, 2002; *J Liu et al.*, 2008; *Wang et al.*, 2008; *Xue et al.*, 2010; *X Zhang*, 2007; *X*
102   *Zhang et al.*, 2008]. The models were usually applied at local scale with a focus on estimating the
103   water budget, with limited attention to groundwater processes and feedbacks to energy related
104   processes. Nevertheless, *Zou et al.* [2015] studied the effects of GW exploitation on land surface
105   processes at the Haihe River Basin located in the NCP. The GW component was conceptualized
106   as a water bucket and the related calculation was based on simple water budget. The over-
107   simplification of GW dynamics in land surface models has been recognized in the last decade,
108   highlighting the lack of representations of lateral GW flow and heat transport [*Bisht et al.*, 2018;
109   *Fang et al.*, 2017; *Zeng et al.*, 2018], which may limit our ability to model not only land surface
110   processes but also land-atmosphere interactions.
111   Recent progress has been made in development of coupled land surface-subsurface models
112   [*Alkhaier et al.*, 2012; *Davison et al.*, 2015; *R. M. Maxwell et al.*, 2011; *R. M. Maxwell and Miller*,
113   2005; *Rahman et al.*, 2015]. In addition, regional or global maps of hydraulic parameters for soils
114   and deep aquifers have become available [*Gleeson et al.*, 2014; *Gleeson et al.*, 2011; *Y G Zhang*

115 *et al.*, 2018] to facilitate integrated modeling at large scales, using models such as ParFlow.CLM
116 over most of the continental US [*R. M. Maxwell and Condon*, 2016] and TerrSysMP over the
117 European CORDEX domain [*Keune et al.*, 2016]. Using an integrated model ParFlow.CLM in the
118 medium-sized Little Washita Basin, *Ferguson and Maxwell* [2011; 2012] studied the effect of
119 irrigation and pumping on land surface water and energy fluxes and compared this effect with that
120 of climate change. Subsequently, in the same basin, *Condon and Maxwell* [2014a; 2014b] studied
121 the system dynamics with a spatio-temporal framework under managed irrigation by coupling
122 ParFlow.CLM with an additional Water Allocation Module. Most recently, *Condon and Maxwell*
123 [2019] studied the sentivity of evapotranspiration and streamflow to groundwater depletion over
124 most of the continental US (CONUS). However, few studies have analyzed the regional GST
125 dynamics under GW pumping using intergrated modeling approach.

126   The overarching goal of this study is to explore the possible effects of GW pumping on land
127 surface processes, especially GST, in the NCP using ParFlow.CLM. The model was first set up
128 over the NCP, then used to study the effects of GW pumping and both pumping and irrigation
129 (P&I) on water and energy related processes, with possible effects on the warming trend in the
130 NCP. In what follows, we introduced the modeling experiments based on ParFlow.CLM and
131 evaluated the baseline scenario by comparing the simulated WTD, GST, sensible heat flux (H),
132 and latent heat flux (LE) with results from previous studies and the JRA-55 reanalysis data
133 products. These variables were selected due to their important roles in land surface-subsurface
134 interactions. Different scenarios were also compared to characterize uncertainties in the modeling.
135 Then the effects of pumping and P&I on WTD and GST were explored. Finally, implications and
136 limitations of this study were summarized.
137

## 2. Integrated modeling in the NCP

2.1. Model description: ParFlow.CLM

140   ParFlow.CLM [*R. M. Maxwell and Miller*, 2005] is an open source, integrated land surface and
141 subsurface model (https://github.com/parflow/parflow) developed by coupling a modified version
142 of the Common Land Model (CLM 3.0) [*Dai et al.*, 2003; *Ferguson et al.*, 2016; *Jefferson and*
143 *Maxwell*, 2015; *Jefferson et al.*, 2017; *R. M. Maxwell and Condon*, 2016] and an integrated surface-
144 subsurface flow model (ParFlow) [*Ashby and Falgout*, 1996; *Jones and Woodward*, 2001; *Kollet*
145 *and Maxwell*, 2006]. ParFlow represents the variably saturated subsurface flow by solving the

146 three-dimensional Richards' equation and integrates it with the overland flow by solving the two-
147 demensional kinematic wave equation and a free-surface boundary condition [*Kollet and Maxwell*,
148 2006]. Replacement of the original one-dimensional vertical flow in CLM by ParFlow overcomes
149 both the shortcoming of the lower flow boundary (e.g., the free drainage) and the limitation in
150 simulating lateral subsurface flow in CLM [*Keune et al.*, 2016; *R. M. Maxwell and Miller*, 2005].
151 At the same time, coupling of ParFlow with CLM improves the simple top boundary used in
152 traditional subsurface flow model like ParFlow, in which snow, surface runoff, soil heating, and
153 root-zone uptake processes are oversimplified or neglected [*R. M. Maxwell and Miller*, 2005].
154 Therefore, ParFlow.CLM can capture more realistic water-energy interactions in the subsurface–
155 land-surface system. The parallel computing capability and terrain following grid in ParFlow make
156 it possible for ParFlow.CLM to be applied at large scale [*Condon and Maxwell*, 2014a]. More
157 details on ParFlow.CLM can be found in many previous studies [*Kollet and Maxwell*, 2008; *R. M.
158 Maxwell and Miller*, 2005]. ParFlow.CLM has been applied to more than a dozen watersheds
159 around the world including the Big Thompson (CO), Klamath (OR), Little Washita (OK), Rur
160 (Germany), San Joaquin (CA), Sante Fe (FL), Chesapeake (MD) and Skjern (Denmark)
161 catchments [*R. M. Maxwell and Condon*, 2016], but it has not been applied and evaluated in the
162 NCP before.

163 **2.2. Modeling domain**

164 The modeling domain (34.45°N–41.00°N, 112.73°E–117.27°E) in this study is shown in
165 Figure 2. The total area is about 467,274 km^2, covering the Beijing Municipality, part of the
166 Tianjing Municipality, and part of the Heibei, Henan, and Shandong Provinces (Figure 2a). The
167 elevation in the study domain ranges from about 3000 m in the northwest Taihang Mountain to
168 near the sea level in the east near the Bohai Sea (Figure 2b, Bohai Sea not shown). The current
169 modeling domain was mostly adopted from the commonly defined NCP region [*Cao et al.*, 2014;
170 *Cao et al.*, 2013; *Qin et al.*, 2013] but slightly modified to simplify the implementation in
171 ParFlow.CLM by using the smallest rectangle to cover the largest area of the NCP. The most active
172 pumping areas, along the Taihang Mountain from Shijiazhuang to Beijing, are well located in the
173 center of the modeling domain, so the boundary effect on the simulation results should be
174 negligible due to the size of the buffer zone [*Keune et al.*, 2016]. Since boundary conditions are
175 not specified at the subsurface topographic boundaries, a rectangular domain was used to move
176 the boundaries away from the study region of interest. Meteorological records showed that, from

177   1980 to 2011, the mean annual precipitation and air temperature were 525 mm and 13.1°C,

178   respectively [*Pei et al.*, 2015].
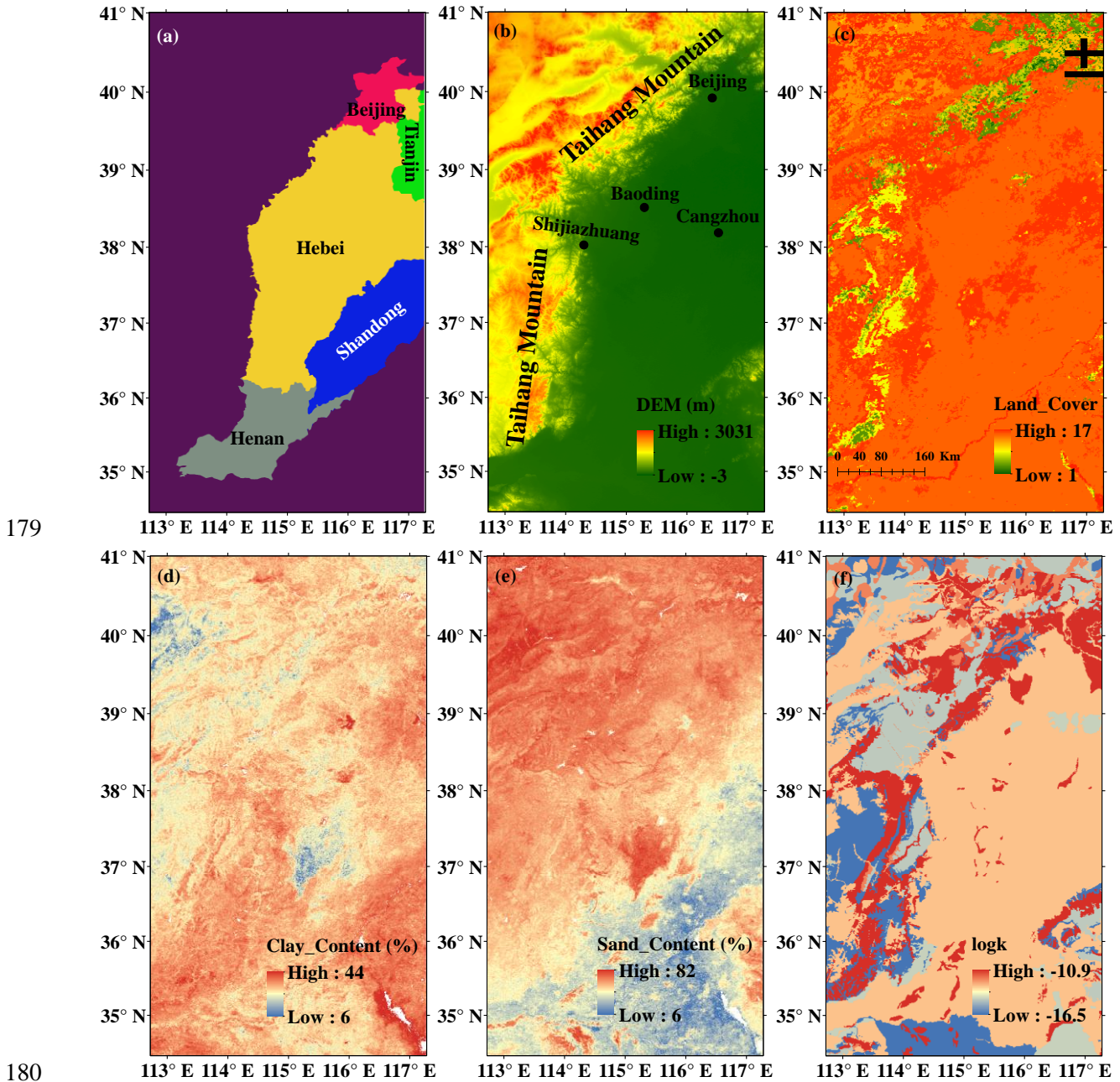
179

180
181   **Figure 2. Administrative regions (a), topography (b), land cover (c), clay content of the surface soil**
182   **(d), sand content of the surface soil (e), and logarithmic permeability of the deep aquifer (f) in the**
183   **NCP modeling domain. 1–17 in the land cover subpanel corresponds to surface types defined by the**
184   **International Geosphere Biosphere Programme (IGBP).**

185

186   **2.3. Subsurface grid**

187   High resolution is necessary to model the effects of well pumping. The cone of depression with

188   WTD increasing from the edge to the center would be averaged to the same WTD if large grid

189   cells are used, which may influence modeling of land surface energy variations that are dependent

190   on the WTD [*Taylor et al.*, 2013]. The subsurface in the study region was divided into 439×799

191   grid cells in the horizontal direction with a resolution of about 1 km. This resolution is higher than

192   the 2 km resolution used in previous regional modeling of the NCP [*Cao et al.*, 2013; *Qin et al.*,

193   2013]. With the terrain following grid, the subsurface was divided into 5 layers in the vertical

194   direction. The thickness of the layers is 0.1, 0.3, 0.6, 1 and 100 m from top to bottom. Thus, the

195   total number of grid cells in the modeling domain is 1,753,805. The setting of vertical thickness is

196   reasonable since the subsurface in the NCP is mainly composed of shallow and deep aquifer groups

197   [*Cao et al.*, 2013], which are relatively independent in terms of hydraulic connections [*Gao*, 2008].

198   The shallow aquifer group is 160 m deep on average [*Cao et al.*, 2013], coinciding with the total

199   thickness of the five layers used in the current study. Only the shallow aquifer group was modeled

200   in this study since it is heavily disturbed by human activities (i.e., pumping and irrigation). This

201   configuration is also consistent with those used in previous studies that have presented good results

202   in CONUS [*R. M. Maxwell and Condon*, 2016; *R. M. Maxwell et al.*, 2015; *R. M. Maxwell et al.*,

203   2016].

204   **2.4. Data descriptions**

205   Topography in the NCP (Figure 2b) was described by the Digital Elevation Model (DEM) of

206   90 m resolution from the Shuttle Radar Topography Mission [*Rabus et al.*, 2003]. Topographic

207   slopes (S_x and S_y) were calculated based on the DEM and then adjusted by the watershed analysis

208   tool in the GRASS Geographic Information System (GIS). The slopes were further modified by

209   the parking lot tests and by the subsequent spin-up processes to ensure connectivity of the streams.

210   Land cover data (Figure 2c) following the classification of the International Geosphere-Biosphere

211   Program (IGBP) from the Global Land Cover Characterization (GLCC) database were

212   downloaded from the USGS website (https://www.usgs.gov/centers/eros). Soil texture and

213   hydraulic parameters (Figures 2d and 2e) in the top 4 layers were from a newly developed global

214   soil map of 1 km resolution [*Y G Zhang et al.*, 2018]. Permeability of the bottom layer (Figure 2f)

215   was from *Gleeson et al.* [2014] with higher resolution than *Gleeson et al.* [2011]. Meteorological

216   forcing data were obtained from the Japanese 55-year Reanalysis project (JRA-55). The forcing

217   data were interpolated to the modeling grid. The 3-hourly forcing data were also linearly

218   interpolated to hourly resolution. All the input data were re-projected to the same world Mercator

219   projected coordinate system and resampled, if necessary, to the same 1 km resolution.

2.5. Boundary and initial conditions

221   We used a free-surface overland flow boundary condition for the land surface and no-flow

222   boundary condition for all other boundaries. No-flow assumption for the lateral and bottom

223   boundaries is reasonable since the buffer zone around the pumping area is large enough, and the

224   shallow aquifer group in the NCP is hydraulically independent from the deep aquifers. For the

225   subsurface (i.e., the ParFlow model), a constant infiltration of 1×10^{-4} m/hour equivalent to the

226   annual precipitation in the NCP and an initial condition of water table at 2 m below the land surface

227   were set. The ParFlow model was spun up until the spatial distribution pattern of pressure head

228   was in quasi-equilibrium. Then the coupled ParFlow.CLM model was spun up for another 2 years

229   to achieve dynamic equilibrium. After the model spin-up, one-year simulations were performed

230   for scenarios 1–5, and two more years were simulated for scenarios 6–7 for the pumping and

231   irrigation experiments (Section 2.6). Forcing data in 1970 was used to represent the

232   predevelopment condition since the extensive GW pumping began in the 1970s. An hourly time

233   step was used in the one-year and two-year simulations producing daily output for analysis.

2.6. Scenario setup

235   The model configuration described above used the best publicly available data and serves as

236   the baseline (scenario 1) in this study. The most uncertain aspects of the modeling are the

237   subsurface permeabilities of soil and aquifer and the atmospheric forcing. Therefore, four

238   additional scenarios were setup by considering different combinations of meteorological forcing

239   and subsurface heterogeneity (Table 1). 2D forcing refers to the spatially variable forcing while

240   1D forcing was defined at the center of the modeling domain and applied to the whole area.

241   Heterogeneous permeabilities were from *Zhang et al*. [2018] in the top soil and from *Gleeson et*

242   *al*. [2014] in the deep aquifer. "Homogeneous" refers to the uniform subsurface with a hydraulic

243   conductivity of 0.6958 m/hour, which is the geometric mean of the hydraulic conductivities in the

244   shallow aquifers of the NCP from *Cao et al*. [2013]. In scenario 5, anisotropy was also considered

245   using a ratio of horizontal to vertical hydraulic conductivity of 10000 [*Cao et al*., 2013].

246   Comparison of the scenarios allows the effects of subsurface properties and meteorological forcing

247   on the regional water and energy processes to be better characterized.

248   After the model was evaluated based on scenarios 1–5, two more scenarios 6 and 7 (Table 1)
249   with pumping and P&I were simulated based on the setting of scenario 1. Groundwater pumping
250   information in the NCP for year 2001 [*Li*, 2013] was used and summarized in Table 2. This
251   information represents the pumping intensity around year 2000 in the NCP. More details about the
252   spatial and temporal variations of pumping in the NCP can be considered in future studies. In this
253   study, groundwater pumping was only conducted in the NCP, i.e., outside the purple area (Figure
254   2a). All the agricultural water in Table 2 was assumed to be for irrigation only in this study.
255   Irrigation was conducted by adding agricultural water to precipitation in the forcing data. In
256   scenario 6, additional quadruple, double, half, and one quarter of the pumping rates were also
257   considered. Increasing rates represent the increasing groundwater demand in the future, while
258   decreasing rates represent the possible effect of smart water management or hydraulic projects,
259   such as the south-to-north water transfer (SNWT) project in the NCP.

260   **Table 1. Scenarios in the subsurface–land-surface modeling in the NCP**

Scenario	Meteorological Forcing	Permeability	Pumping	Irrigation
1 (Baseline)	2D	Heterogeneous	No	No
2	2D	Homogeneous	No	No
3	1D	Heterogeneous	No	No
4	1D	Homogeneous	No	No
5	2D	Heterogeneous and anisotropy	No	No
6	2D	Heterogeneous	Yes	No
7	2D	Heterogeneous	Yes	Yes

261

262   **Table 2. Groundwater pumping in shallow aquifers in the NCP**

Administrative Regions	Total Pumping (10^8 m³/year)	Area (10^4 km²)	Pumping Rate (m/hour)	Agricultural Water (10^8 m³/year)
Beijing	26.44	1.04	2.89×10^{-5}	13.38
Tianjin	1.06	1.76	6.87×10^{-7}	0.99
Hebei	118.53	11.41	1.19×10^{-5}	99.81
Henan	28.04	2.63	1.22×10^{-5}	23.36
Shandong	15.93	4.79	3.79×10^{-6}	10.10

3. Results and Discussion

3.1. Model evaluation

3.1.1. Water table depth

The simulated annual averaged WTD in 1970 in the baseline is shown in Figure 3a. Simulated WTD is generally 1 m in the plain area but reaches more than 60 m in the mountain areas. The WTD in the plain area of the NCP during predevelopment was estimated at 0–3 m [*Cao et al.*, 2013; *Fei et al.*, 2009]. Thus, the simulated WTD is within the range of the predevelopment condition. Compared to scenario 2 (Figure 3b), the WTD is more controlled by the DEM for a homogeneous subsurface but it is adjusted by the subsurface heterogeneity in scenario 1. Although the WTD in mountain areas is generally large, it can be much smaller if the aquifer has low permeability (e.g., area indicated by the red circle in Figure 3a). Some previous studies considered either an exponential decay of permeabilities with depth [*Jiang et al.*, 2009] or a vertical anisotropy [*Cao et al.*, 2013]. Scenario 5 with vertical anisotropy has much smaller WTD (Figure S1c).

Scenario 1 with homogeneous permeability in the vertical direction also shows a shift of WTD to 0 m although it ranges between 0–3 m, indicating that the parameters in *Zhang et al.* [2018] and/or *Gleeson et al.* [2014] were likely underestimated. Shallower WTD was also estimated in previous studies [*Fan et al.*, 2013; *R. M. Maxwell et al.*, 2015], which suggested that the bias may be mainly due to GW pumping that was not considered in the simulation. Similarly, GW pumping already happened in the 1970s in the NCP, which might be another reason for the shallower WTD simulated in scenario 1 compared to observations. In general, variations of WTD, decreasing from piedmont plain to coastal plain, are well captured in the simulation. The ~1m WTD in the plain areas lies in the sensitive WTD range proposed by *Kollet and Maxwell* [2008] and *Ferguson and Maxwell* [2011], in which GW dynamics have larger influence on land surface processes. Following this argument of the sensitive WTD range, long-term GW pumping increasing WTD from 1 m during predevelopment to more than 10 m today may have greatly altered the water and energy budgets in the NCP, which is explored in section 3.2.
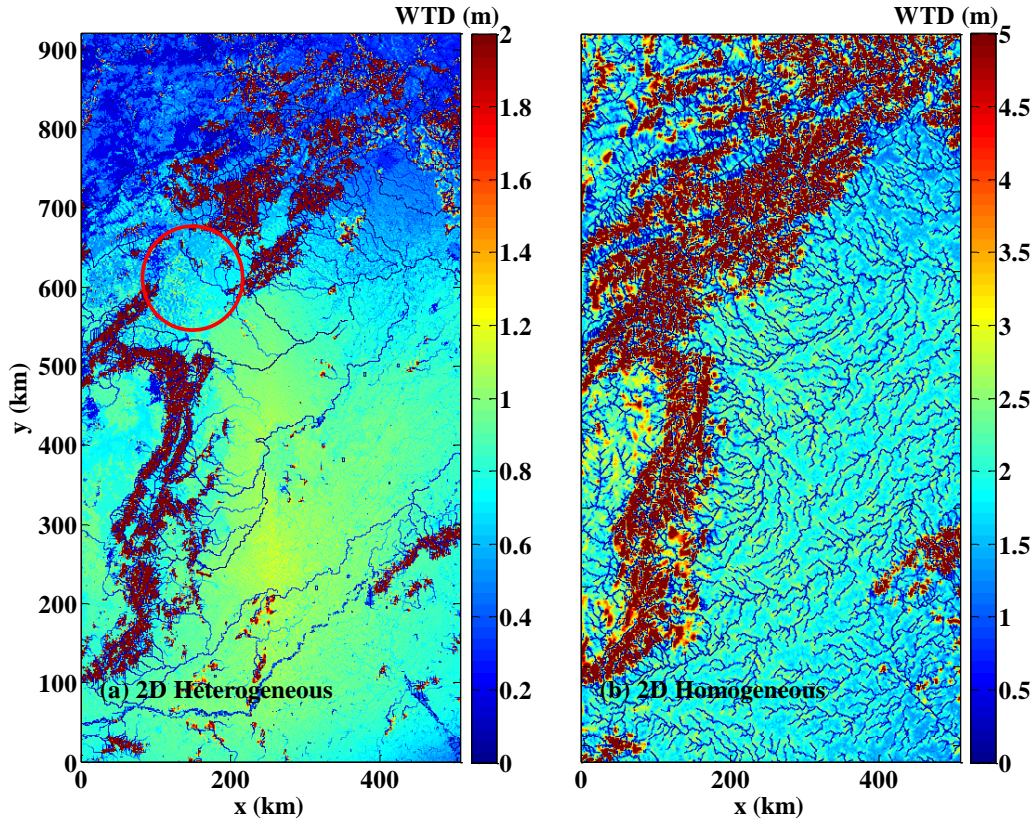
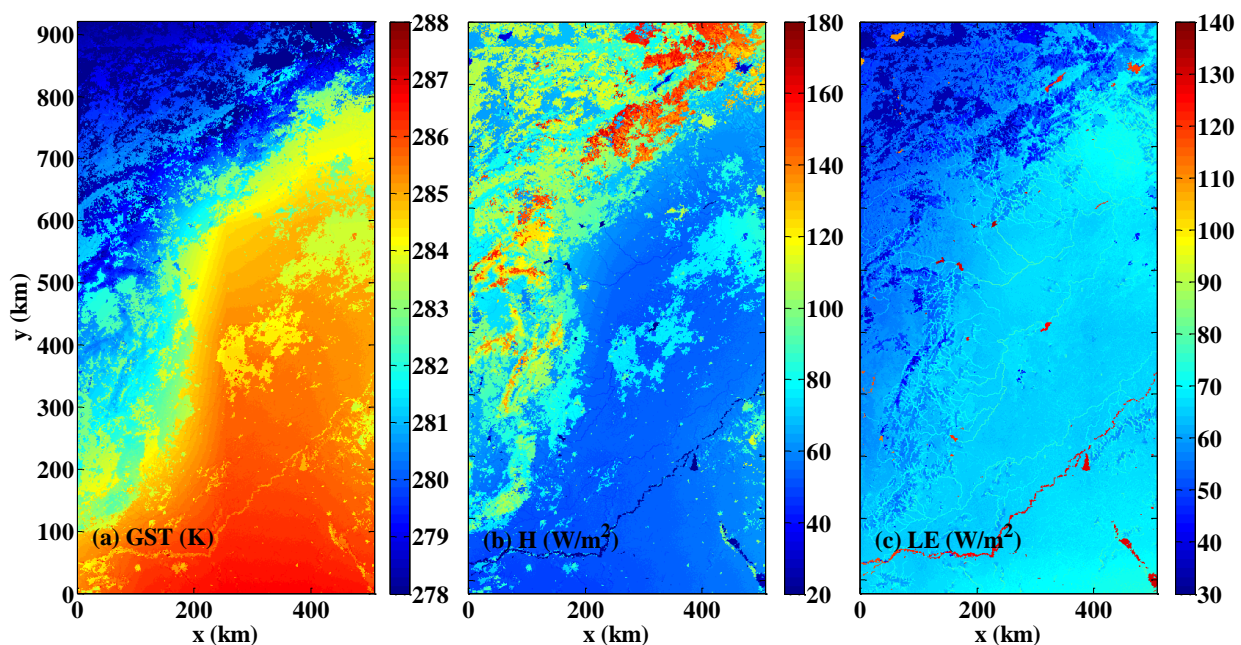**Figure 3. Simulated annual averaged WTD in 1970 for scenarios 1 and 2.**

3.1.2. Ground surface temperature and surface heat fluxes

The simulated spatial distribution of annual averaged GST in 1970 (Figure 4a) is consistent with that of the JRA-55 reanalysis data (Figure 5a). GST decreases from about 288 K in the south to about 278 K in the northwest. There is a clear difference in GST between the plain and mountain areas due to topography. Seasonal cycle of the simulated GST also matches the trends of JRA-55, showing only a small cold bias (Figure 6a). One possible reason could be the lack of pumping in scenario 1 that is in contrast to the reality in 1970, which will be further studied in section 3.2. The capability to capture the temporal and spatial variations of GST supports the use of the model to study the effects of GW pumping on GST in the NCP.

Spatial distribution of the simulated sensible (H) and latent (LE) heat fluxes are shown in Figure 4. A narrow band with higher H is simulated between the mountain and plain areas. LE has a more uniform distribution, with slightly higher values in the northeast and south. These spatial patterns are quite consistent with those of JRA-55 shown in Figure 5. The general temporal variability of H and LE is comparable to that of JRA-55. It is also noted that 1D forcing produces higher GST than 2D forcing (Figure S2a). Correspondingly, lower H and higher LE are obtained

307   by using 1D relative to 2D forcing (Figure S2). 2D forcing generally produces more realistic results

308   (Figure S2), suggesting the importance to represent the spatial variability of atmospheric forcing

309   in the NCP region. With 1D forcing, energy related variables (GST, H, and LE) exhibit minimal

310   difference under different subsurface heterogeneities (Figure S2). Whereas, the WTD is more

311   controlled by the subsurface heterogeneity than the forcing (Figures 3 and S1).
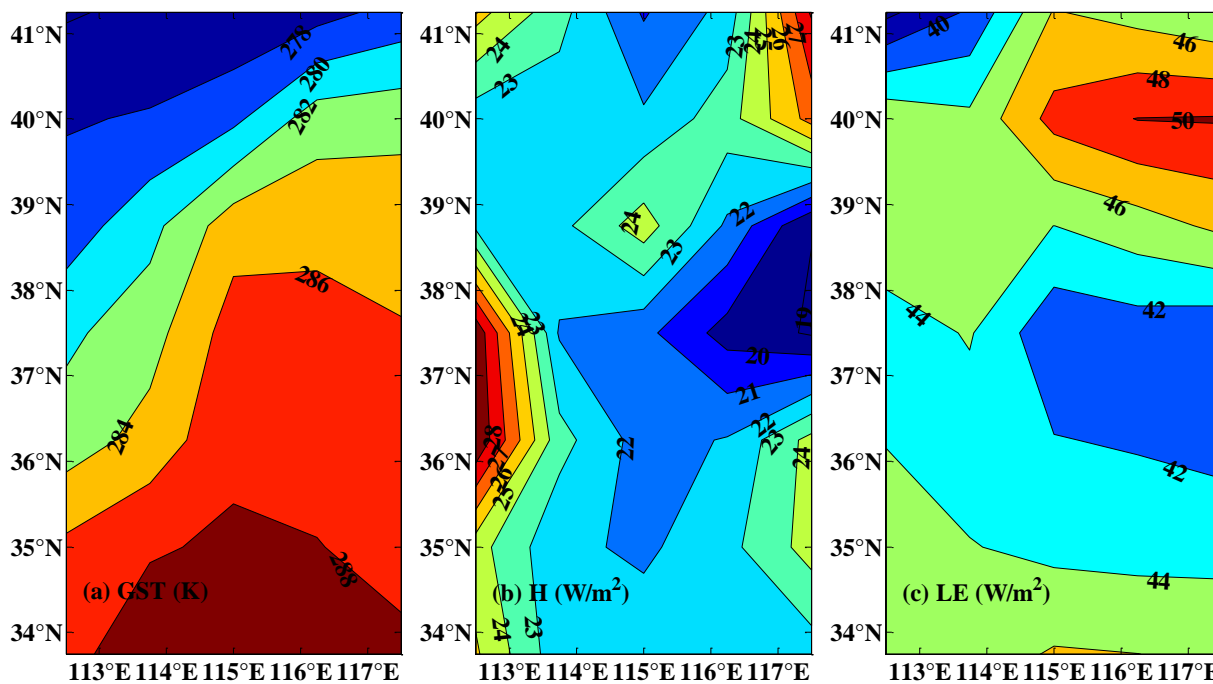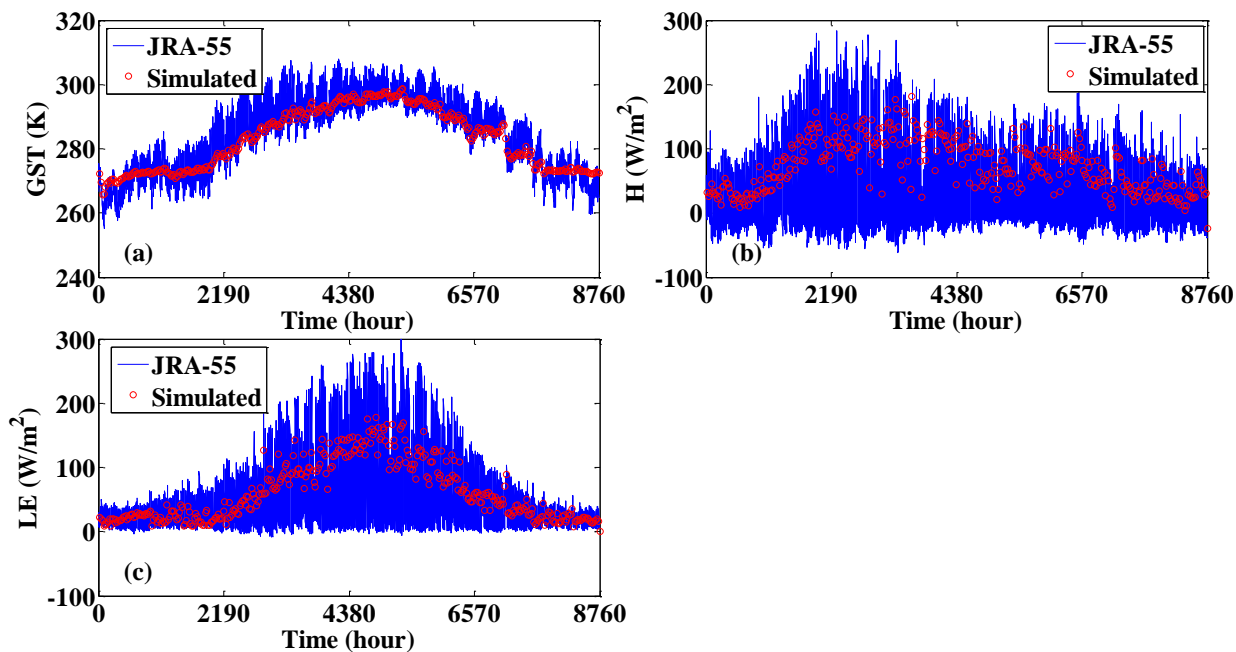

312

313   **Figure 4. Simulated annual averaged GST, H, and LE in 1970 for scenario 1.**

314

315

316

Figure 5. Annual averaged GST, H, and LE in 1970 based on the JRA-55 data of 3-hours resolution
in time and 1.25-degree resolution in space.

319

320

Figure 6. Spatially averaged variations of GST, H, and LE with time in 1970 for scenario 1.

322
323
324
325

3.2. Effects of groundwater pumping and irrigation

Evaluation of the simulated water and energy components discussed in section 3.1 indicates the feasibility to conduct GW pumping and P&I using the ParFlow.CLM model. Increase of WTD (ΔWTD) after one and two years of pumping is shown in Figure 7. The most obvious increase occurs in Beijing, western Hebei, and Henan, while smaller increase in WTD is found in Tianjin and Shandong due to the smaller pumping rates (Table 2). However, WTD in northern Hebei increases less than other parts of Hebei (red circles in Figure 7), which could be due to the lateral flow recharge from nearby Tianjin and Shandong with less pumping. Besides, the Taihang Mountain next to this area with higher permeability (Figure 2f) might also induce lateral flow from mountain area toward the east. The lateral flow simulated in these areas have been confirmed by field observations (Figure S3) [*Li*, 2013]. In Figure S3, WTD is larger in Beijing and along the Taihang mountain, then decreases toward Shandong and Tianjin in the east, and is relatively smaller in northern Hebei. These consistencies between the modeling results and observations further demonstrate the fidelity of the model.

WTD in the plain areas increases by less than 0.5 m after one year of pumping, and by almost 1 m in some places such as Beijing after 2 years of pumping. The rate of WTD increase (~ 0.5 m/year) is higher than that reported (~ 0.3 m/year) in *Cao et al*. [2013] because they calculated an average rate for the whole NCP without considering the spatial variability as shown in Figure 7. In addition, ignoring irrigation might have exaggerated the impacts of pumping on WTD in our simulation. However, considering the uneven spatial distribution of the cone of depression, the rate could also be underestimated by our model. For example, the WTD increase for the cone of depression in Baoding from 1975 to 1985 is more than 1.6 m per year [*Li*, 2013]. With irrigation, WTD increase became slow and the maximum increase of WTD after two years of simulation was about 0.5 m, which is more consistent with *Cao et al*. [2013]. In general, the spatial and temporal variations of WTD are reasonable in the pumping and irrigation experiments.

Change of monthly averaged GST after one year of pumping is shown in Figure 8, and that after 2 years of pumping is shown in Figure S4. Notably, obvious changes of GST only occurred in the area with pumping. GST in the plain area is less disturbed by pumping from December to February. GST increases from April to July mainly in Beijing and northern Hebei, while it decreases from September to November in Beijing, western Hebei and Henan. Of particular interest is the larger increase of GST in summer than the decrease of GST in winter, leading to an

357   increasing annual average GST. Taking Beijing for example, the average and maximum increase

358   of GST in summer (May to July) are 0.23 and 1.06 °C respectively; while the average and

359   maximum decrease of GST in winter (September to Novemeber) are 0.11 and 0.69 °C respectively.

360   *H Zhang et al.* [2016] reported an increase in annual mean GST of 2.07–4.04 and 0.66–2.21 °C in

361   northern and southern China (1962–2011), respectively. The maximum increase of GST per year

362   due to pumping modeled in this study is over 1℃, suggesting potentially a significant contribution

363   of pumping to the reported GST change. An increase in GST of about 2°C for cropland associated

364   with WTD ranging from 2 to 5 m was reported by *Kollet and Maxwell* [2008]. In addition, the

365   increase in GST in a one-year simulation was 1–3°C as reported by *R. M. Maxwell and Kollet*

366   [2008] under prescribed hot and dry climatic condition in the future. Our results are comparable

367   to the GST changes reported in previous studies.

368   In addition, by changing the pumping rates in scenario 6, nonlinear variations of ΔGST were

369   obtained. Taking June in Beijing as an example, the average ΔGST with double pumping rate

370   scenario (0.61℃) is about twice as large as the ΔGST with normal pumping rate (0.33℃). In

371   comparison, when the pumping rate is reduced to half, the average ΔGST becomes about one third

372   (0.10 ℃) of that under normal rate (0.33℃). More importantly, one year of pumping with double

373   rate generated higher ΔGST than two years of pumping with normal rate, which can be observed

374   in Figure S5, such as the increase of GST in May and the decrease of GST in October. Therefore,

375   moderate pumping rate under sound water management is important for sustainability of water

376   resources and sustainable development of ecological environment. With irrigation, the increase

377   and decrease of GST are obviously alleviated (Figures 9 and S6), but cannot be completely

378   eliminated. Applying pumping and irrigation to crop areas in the Washita watershed, *Ferguson*

379   *and Maxwell* [2011] found that pumping led to an increase of WTD over 15% of the watershed

380   area while irrigation led to a decrease of WTD in only 1.6% of the watershed, which also indicates

381   the limited compensation of irrigation. As irrigation provides water needed for crop growth, a large

382   fraction of irrigation water supply is balanced by increases in evapotranspiration, so irrigation has

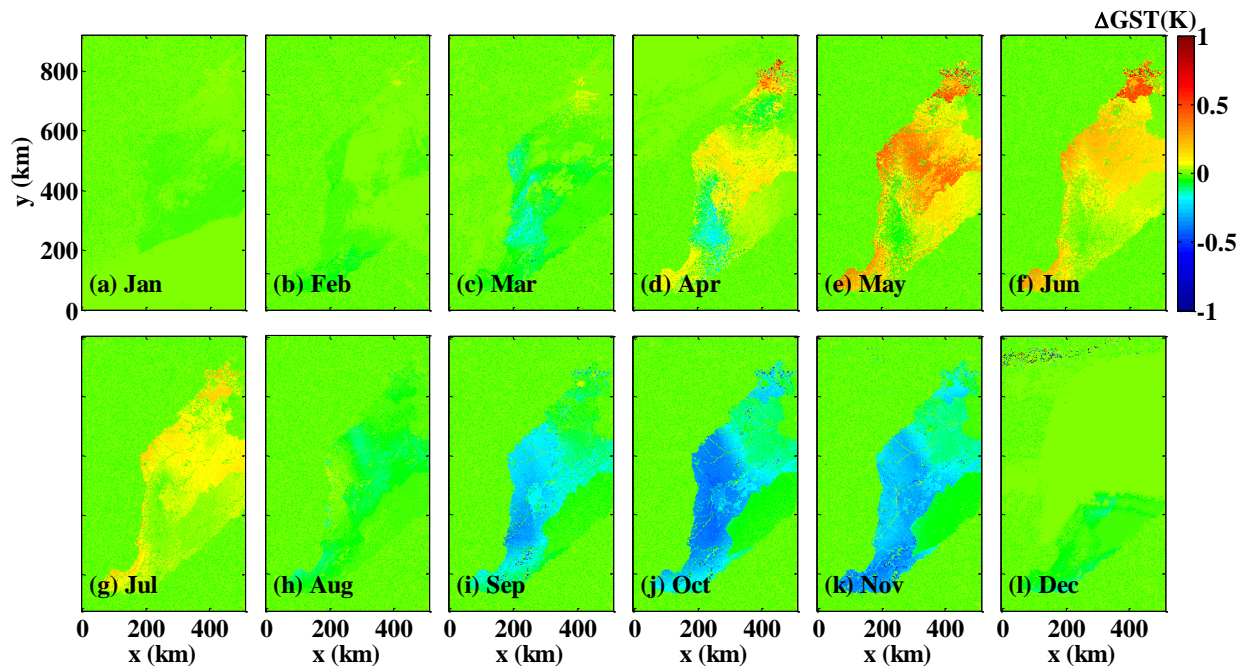383   smaller effect on WTD than pumping.

384
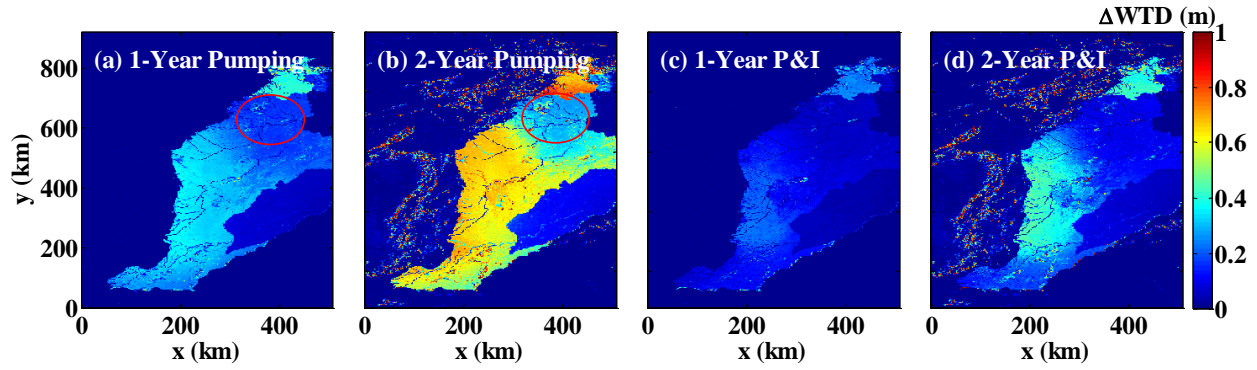
Figure 7. Simulated change of annual averaged WTD after one year of pumping (a), 2 years of pumping (b), one year of pumping and irrigation (c), and 2 years of pumping and irrigation (d).
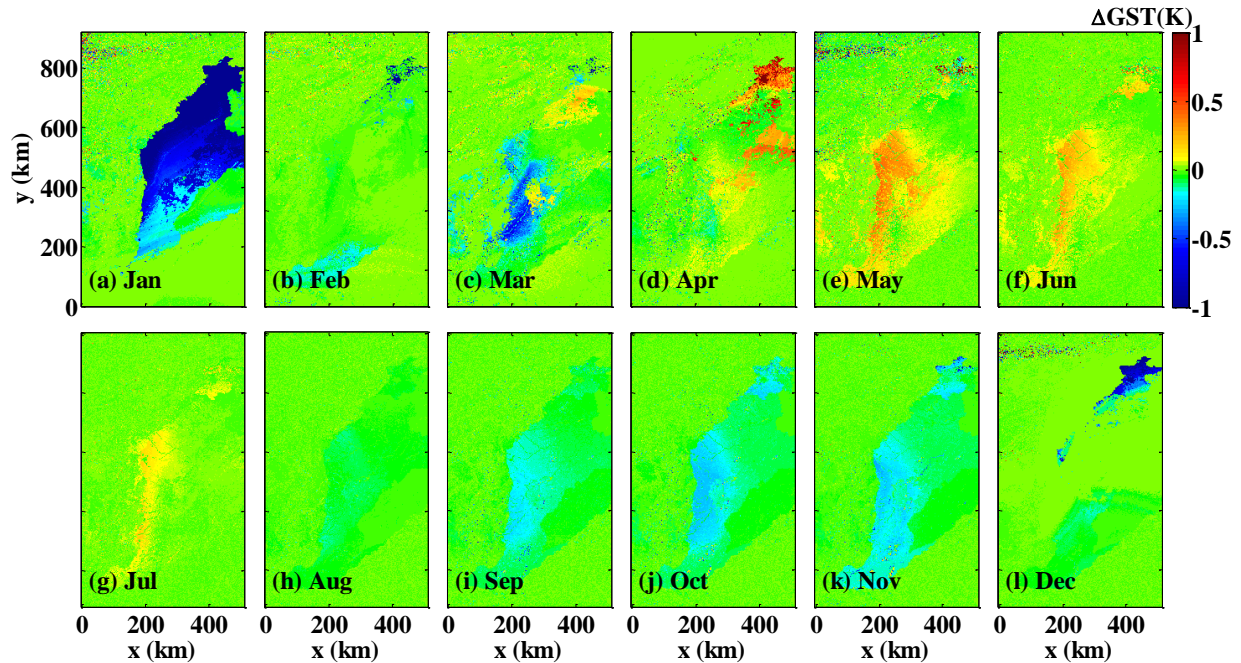
387

388

Figure 8. Simulated change of monthly averaged GST after one year of pumping.

390

391

Figure 9. Simulated change of monthly averaged GST after one year of pumping and irrigation.

3.3. Mechanisms and implications

Soil heat transport in CLM 3.0 is solved by the heat balance and conduction equations written as (1) and (2), respectively [*Dai et al.*, 2003; *Kollet et al.*, 2009], in the vertical direction:

$$c\frac{\partial T}{\partial t} = -\frac{\partial F}{\partial z} + S \tag{1}$$

$$F = -\lambda\frac{\partial T}{\partial z} \tag{2}$$

where c is the volumetric heat capacity; T is the soil temperature, which is GST at the land surface; t is time; F is the heat flux and at the land surface, it is the ground heat flux (G); z is the vertical distance from the soil surface and is positive downward; S is the latent heat of phase change; and λ is the thermal conductivity. As the top boundary condition in modeling heat transport in the subsurface, G might be a factor inducing variations in GST. The monthly averaged changes of LE, H, and G after one year of pumping are shown in Figures S7, S8, and 10, respectively. With increasing WTD by pumping, LE decreases and H increases, consistent with the general subsurface–land-surface feedback mechanism reflected by the increase of Bowen ratio [*Keune et al.*, 2016; *Pal and Eltahir*, 2001]. The increase of G in summer from April to July may contribute to the increase of GST at the same time. However, increasing G is also simulated while GST decreases in autumn and winter from September to November. Considering that soil moisture

411 decreases with pumping, the volumetric heat capacity decreases [*Abu-Hamdeh*, 2003] so the heat

412 storage/release capacity of the subsurface decreases. Therefore, in summer, heat flux into the

413 subsurface combined with reduced heat storage capacity increase GST. In winter, reduced heat

414 flux released from the subsurface due to the reduced heat storage in summer leads to the decrease

415 in GST even though G increases.
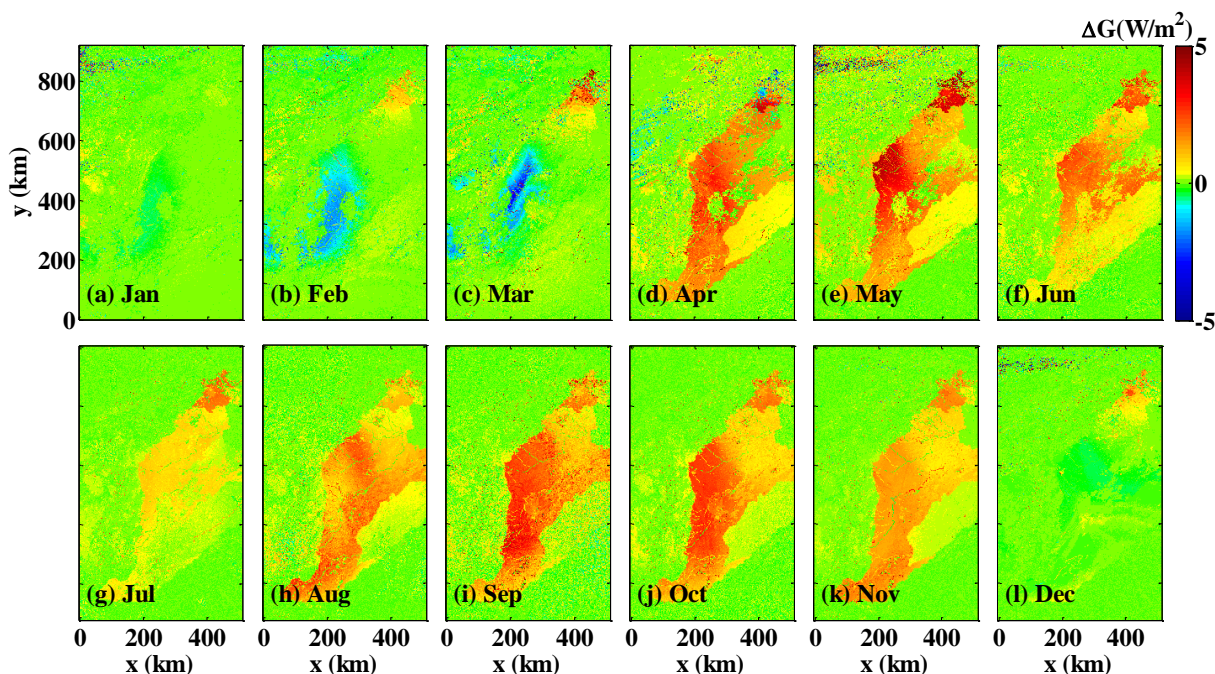
Figure 10. Simulated change of monthly averaged G after one year of pumping.

419   Previous studies suggested that WTD may have larger influence on land surface heat fluxes

420 when it is within a specific range of depths [e.g., *Maxwell and Kollet*, 2008]. Often GW supplies

421 moisture for surface heat fluxes when WTD is shallow. In contrary, when the water table is too

422 deep, GW has little influence on soil moisture that contributes to surface heat fluxes. The

423 thresholds of such range was well-stated by numerous previous case studies [*Ferguson and*

424 *Maxwell*, 2010; *Kollet and Maxwell*, 2008; *Reed M. Maxwell et al.*, 2007; *Szilagyi et al.*, 2013]

425 and summarized as 1–10 m [*Ferguson and Maxwell*, 2011]. In *Condon et al.* [2013], possible

426 influencing factors on the critical depth range were sysmeitcally studied. Results revealed that the

427 critical range does not vary significantly with subsurface parameters. Though land cover and soil

428 types affect the shape of the relationship between WTD and land surface heat fluxes, the bulk

429 range of the critical depth stays the same. Hence, the 1–10 m critical depth range in [*Ferguson and*

430   *Maxwell*, 2011] was aopted for the following discussion. Therefore, with the 0.5 m increase of

431   WTD per year estimated due to pumping, WTD may continue to increase from the 1970, i.e., pre-

432   pumping condition, for about 20 years until the average WTD drops below 10 m. Hence pumping

433   could have influenced GST for one decade or two. Considering the uneven WTD-distribution of a

434   depression-cone, the pumping influence can last longer time than 20 years regionally. Considering

435   the nonlinear change of GST with WTD discussed in section 3.2, the increase of GST should be

436   faster in the beginning and gradually slow down. Generally, the subsurface acts as a buffer to heat

437   fluxes at the land surface but long-term pumping can gradually weaken and finally invalidate this

438   buffer when the water table becomes too deep. The weakened buffer can result in higher temporal

439   variability of GST, i.e., colder winter and hotter summer. Although irrigation alleviates the impacts

440   of pumping by increasingsoil moisture at the land surface, it cannot completely eliminate the

441   pumping effect.

442   **3.4. Limitations and future work**

443   Our modeling and analyses could be potentially improved in a few directions, although we do

444   not expect them to have large influence on our major conclusions. More information on the

445   temporal and spatial variations of pumping and irrigation in the NCP during the past 60 years may

446   be used to further constrain the model setup in future studies. The NCP is also influenced by

447   urbanization, which deserves attention when attributing changes in GST in the region. For example,

448   land use data of the NCP in 2003 [*Cao et al.*, 2014] and 2009 [*Pei et al.*, 2015] illustrates that

449   urban regions scattered among croplands have expanded gradually. Urban expansion can alter the

450   spatial distribution of irrigation regions by reducing their sizes and fragmenting their coverage.

451   Meanwhile, a depression cone can continue to expand from its center located mainly in the

452   irrigation regions to a much broader area. Urban areas located outside the irrigation regions may

453   sit on top of some cones of depression far away. Near the edges of the groundwater cones of

454   depression, the shallow WTD may stay within the critical zone (WTD of 1–10 m), so the effect of

455   pumping can be significant when irrigation is not regulated. In this study, sprinkler irrigation is

456   applied by adding the irrigation water to precipitation. However, flood irrigation is the most

457   popular irrigation method in the NCP [*Cao et al.*, 2013]. Flood irrigation has lower water

458   utilization efficiency [*Kendy et al.*, 2007; *Scanlon et al.*, 2012] than sprinkler irrigation, which can

459   lead to larger increase in GST than what we obtained in this study. Flood irrigation has not been

460   implemented in ParFlow.CLM so that future work should consider modeling different irrigation

461   methods to allow investigation into their specific impacts [*Delos Reyes and Schultz*, 2019; *Leng et*
462   *al.*, 2017].

463   Future work could also improve modeling of land surface processes as heat transport in CLM
464   is described using a one-dimensional vertical model, while in the ParFlow groundwater flow is
465   modeled using the three-dimensional Richards' equation. This approach is reasonable for
466   modeling energy and water fluxes in regions in an energy limited regime and human influence is
467   small. However, with human activities such as GW pumping, horizontal temperature gradient may
468   be induced, so horizontal heat transport should not be neglected. Other shortcomings of the
469   modeling approach include the limited soil depth and the simple lower boundary condition
470   implemented in CLM for heat transport. *Davison et al.* [2015] investigated the sensitivity of GST
471   simulations to soil depth using aquifers of 2 m and 8 m depth in 100 days of simulation under
472   prolonged drought condition. Although GST shows no difference between the two settings, deep
473   soil temperature (> 1 m) is higher for the simulation with aquifer depth of 2 m. With longer
474   simulations, the difference of deep soil temperature becomes greater and propagates to the land
475   surface so GST may be expected to be different in the two settings after 100 days of simulation.
476   Since GW pumping has been practiced in the NCP for more than 60 years, future studies should
477   also consider increasing the model soil depth for heat transport. The critical depth of WTD
478   proposed by *Kollet and Maxwell* [2008] was based on a one-year simulation, showing that the
479   deficiency related to heat transport at depth can be neglected.

480

4. Conclusions

482   In this study, integrated land surface-subsurface modeling of the NCP was performed using
483   ParFlow.CLM. The model produced realistic water and energy dynamics that are highly consistent
484   with those in previous studies and from the JRA-55 data, respectively. Both the spatial and
485   temporal variations of water and energy processes were well captured by the integrated model.
486   Based on a suite of numerical experiments, the effects of GW pumping and combined pumping
487   and irrigation on water and energy were explored, with a focus on the ground surface temperature
488   (GST) which was rarely discussed in previous studies. Results show significant effects of GW
489   pumping on the GST in the NCP. Generally, the subsurface acts as a buffer to heat fluxes at the
490   land surface, but long-term pumping can gradually weaken and finally invalidate this buffer. This

491 results in higher temporal variability of GST, featuring hotter summer and colder winter. Increased
492 spatial variabilities of GST was also captured.

493 Considering that changes of WTD can significantly affect surface heat fluxes for WTD roughly
494 in the range of 1–10 m, the 0.5 m/year increase of WTD can continuously increase GST for at least
495 20 years based on the 1970 average WTD in the NCP. If the uneven WTD distribution of
496 depression cones is also considered, this influence could last until the WTD in the whole NCP
497 increases by over 10 m, which may take longer than 20 years. In addition, GST is expected to
498 increase faster at the beginning and gradually slow down due to the nolinear variations of GST
499 with WTD. Irrigation alleviates this situation by increasing soil moisture at the land surface but it
500 cannot completely eliminate the pumping effect. Considering the spatial and temporal variations
501 of pumping and irrigation, urbanization, and how irrigation was modeled in this study, the effect
502 of irrigation might be overestimated.

503 This study aimed to build a realistic modeling platform to understand the water and energy
504 cycles and their interactions in a subsurface–land-surface system. Hence no efforts were devoted
505 to establishing a calibrated model to fit the historical data or to predict future changes. Unlike
506 previous studies that modeled the surface and subsurface as separated systems in the NCP, the
507 coupled ParFlow.CLM model provides an important tool for more investigations of pumping and
508 irrigation in the context of climate change in the future. GW pumping has already been a global
509 problem and occurs not only in the NCP but also in northwestern India, Middle East, the U.S. High
510 Plains [*Famiglietti*, 2014] and other regions. Hence the results of this study may have implications
511 for other regions with GW depletion and motivate the need to investigate the role of GW pumping
512 in regional climate change.

513

521

References

A, D., K. Xiong, W. J. Zhao, Z. N. Gong, R. Jing, and L. Zhang (2016), Temporal Trend of Climate Change and Mutation Analysis of North China Plain During 1960 to 2013 [in Chinese with English abstract], *Scientia Geographica Sinica*, *36*(10), 1555-1564.

Abu-Hamdeh, N. H. (2003), Thermal properties of soils as affected by density and water content, *Biosyst Eng*, *86*(1), 97-102, doi:10.1016/S1537-5110(03)00112-0.

Alkhaier, F., G. N. Flerchinger, and Z. Su (2012), Shallow groundwater effect on land surface temperature and surface energy balance under bare soil conditions: modeling and description, *Hydrol Earth Syst Sc*, *16*(7), 1817-1831, doi:10.5194/hess-16-1817-2012.

Ashby, S. F., and R. D. Falgout (1996), A parallel multigrid preconditioned conjugate gradient algorithm for groundwater flow simulations, *Nucl Sci Eng*, *124*(1), 145-159.

Bisht, G., W. J. Riley, H. M. Wainwright, B. Dafflon, F. M. Yuan, and V. E. Romanovsky (2018), Impacts of microtopographic snow redistribution and lateral subsurface processes on hydrologic and thermal states in an Arctic polygonal ground ecosystem: a case study using ELM-3D v1.0, *Geosci Model Dev*, *11*(1), 61-76, doi:10.5194/gmd-11-61-2018.

Cao, G. L., D. M. Han, and X. F. Song (2014), Evaluating actual evapotranspiration and impacts of groundwater storage change in the North China Plain, *Hydrol Process*, *28*(4), 1797-1808, doi:10.1002/hyp.9732.

Cao, G. L., C. M. Zheng, B. R. Scanlon, J. Liu, and W. P. Li (2013), Use of flow modeling to assess sustainability of groundwater resources in the North China Plain, *Water Resour Res*, *49*(1), 159-175, doi:10.1029/2012wr011899.

Condon, L. E., and R. M. Maxwell (2014a), Feedbacks between managed irrigation and water availability: Diagnosing temporal and spatial patterns using an integrated hydrologic model, *Water Resour Res*, *50*(3), 2600-2616, doi:10.1002/2013wr014868.

Condon, L. E., and R. M. Maxwell (2014b), Groundwater-fed irrigation impacts spatially distributed temporal scaling behavior of the natural system: a spatio-temporal framework for understanding water management impacts, *Environ Res Lett*, *9*(3), doi:Artn 03400910.1088/1748-9326/9/3/034009.

Condon, L. E., and R. M. Maxwell (2019), Simulating the sensitivity of evapotranspiration and streamflow to large-scale groundwater depletion, *Sci Adv*, *5*(6), doi:ARTN eaav457410.1126/sciadv.aav4574.

Condon, L. E., R. M. Maxwell, and S. Gangopadhyay (2013), The impact of subsurface conceptualization on land energy fluxes, *Adv Water Resour*, *60*, 188-203, doi:10.1016/j.advwatres.2013.08.001.

Cui, Y., Y. Wang, J. Shao, Y. Chi, and L. Lin (2009), Research on groundwater regulation and recovery in North China Plain after the implementation of south-to-north water transfer [in Chinese with English abstract], *Resour. Sci.*, *31*(3), 382-387.

Dai, Y. J., et al. (2003), The Common Land Model, *B Am Meteorol Soc*, *84*(8), 1013-1023, doi:10.1175/Bams-84-8-1013.

Davidson, E. A., I. A. Janssens, and Y. Q. Luo (2006), On the variability of respiration in terrestrial ecosystems: moving beyond Q(10), *Global Change Biol*, *12*(2), 154-164, doi:10.1111/j.1365-2486.2005.01065.x.

Davison, J. H., H. T. Hwang, E. A. Sudicky, and J. C. Lin (2015), Coupled atmospheric, land surface, and subsurface modeling: Exploring water and energy feedbacks in three-dimensions, *Adv Water Resour*, *86*, 73-85, doi:10.1016/j.advwatres.2015.09.002.

Delos Reyes, M. L. F., and B. Schultz (2019), Modernization of National Irrigation Systems in the Philippines: Linking Design, Operation and Water Supply, *Irrigation and Drainage*, *68*(1), 59-66, doi:10.1002/ird.2260.

Famiglietti, J. S. (2014), The global groundwater crisis, *Nat Clim Change*, *4*(11), 945-948.

Fan, Y., H. Li, and G. Miguez-Macho (2013), Global Patterns of Groundwater Table Depth, *Science*, *339*(6122), 940-943, doi:10.1126/science.1229881.

Fang, Y. L., L. R. Leung, Z. R. Duan, M. S. Wigmosta, R. M. Maxwell, J. Q. Chambers, and J. Tomasella (2017), Influence of landscape heterogeneity on water available to tropical forests in an Amazonian

572   catchment and implications for modeling drought response, *J Geophys Res-Atmos*, *122*(16), 8410-
573   8426, doi:10.1002/2017jd027066.

574   Fei, Y. H., J. X. Miao, Z. J. Zhang, Z. Y. Chen, H. B. Song, and M. Yang (2009), Analysis on Evolution of
575   Groundwater Depression Cones and Its Leading Factors in North China Plain [in Chinese with English
576   abstract], *Resources Science*, *31*(3), 394-399.

577   Ferguson, I. M., J. L. Jefferson, R. M. Maxwell, and S. J. Kollet (2016), Effects of root water uptake
578   formulation on simulated water and energy budgets at local and basin scales, *Environ Earth Sci*, *75*(4),
579   doi:ARTN 31610.1007/s12665-015-5041-z.

580   Ferguson, I. M., and R. M. Maxwell (2010), Role of groundwater in watershed response and land surface
581   feedbacks under climate change, *Water Resour Res*, *46*.

582   Ferguson, I. M., and R. M. Maxwell (2011), Hydrologic and land-energy feedbacks of agricultural water
583   management practices, *Environ Res Lett*, *6*(1), doi:Artn 01400610.1088/1748-9326/6/1/014006.

584   Ferguson, I. M., and R. M. Maxwell (2012), Human impacts on terrestrial hydrology: climate change versus
585   pumping and irrigation, *Environ Res Lett*, *7*(4), doi:Artn 04402210.1088/1748-9326/7/4/044022.

586   Gao, Y. (2008), Study on Groundwater Hydraulic Connection in Different Aquifers under mass Pumped
587   Conditions in Typical Area North China Plain, 147 pp, Chinese Academy of Geological Sciences,
588   Beijing.

589   Gleeson, T., N. Moosdorf, J. Hartmann, and L. P. H. van Beek (2014), A glimpse beneath earth's surface:
590   GLobal HYdrogeology MaPS (GLHYMPS) of permeability and porosity, *Geophys Res Lett*, *41*(11),
591   3891-3898, doi:10.1002/2014gl059856.

592   Gleeson, T., L. Smith, N. Moosdorf, J. Hartmann, H. H. Durr, A. H. Manning, L. P. H. van Beek, and A. M.
593   Jellinek (2011), Mapping permeability over the surface of the Earth, *Geophys Res Lett*, *38*, doi:Artn
594   L0240110.1029/2010gl045565.

595   Harada, Y., H. Kamahori, C. Kobayashi, H. Endo, S. Kobayashi, Y. Ota, H. Onoda, K. Onogi, K. Miyaoka,
596   and K. Takahashi (2016), The JRA-55 Reanalysis: Representation of Atmospheric Circulation and
597   Climate Variability, *J Meteorol Soc Jpn*, *94*(3), 269-302, doi:10.2151/jmsj.2016-015.

598   Hu, Y. K., J. P. Moiwo, Y. H. Yang, S. M. Han, and Y. M. Yang (2010), Agricultural water-saving and
599   sustainable groundwater management in Shijiazhuang Irrigation District, North China Plain, *J. Hydrol.*,
600   *393*(3-4), 219-232.

601   Jefferson, J. L., and R. M. Maxwell (2015), Evaluation of simple to complex parameterizations of bare
602   ground evaporation, *J Adv Model Earth Sy*, *7*(3), 1075-1092, doi:10.1002/2014ms000398.

603   Jefferson, J. L., R. M. Maxwell, and P. G. Constantine (2017), Exploring the Sensitivity of Photosynthesis
604   and Stomatal Resistance Parameters in a Land Surface Model, *J Hydrometeorol*, *18*(3), 897-915,
605   doi:10.1175/Jhm-D-16-0053.1.

606   Jia, J., and C. Liu (2002), Groundwater dynamic drift and response to different exploitation in the North
607   China Plain: A case study of Luancheng County, Hebei Province [in Chinese with English abstract],
608   *Acta Geogr. Sin.*, *57*(2), 201-209.

609   Jiang, X. W., L. Wan, X. S. Wang, S. M. Ge, and J. Liu (2009), Effect of exponential decay in hydraulic
610   conductivity with depth on regional groundwater flow, *Geophys Res Lett*, *36*, doi:Artn
611   L2440210.1029/2009gl041251.

612   Jones, J. E., and C. S. Woodward (2001), Newton-Krylov-multigrid solvers for large-scale, highly
613   heterogeneous, variably saturated flow problems, *Adv Water Resour*, *24*(7), 763-774.

614   Kang, S., and E. A. B. Eltahir (2018), North China Plain threatened by deadly heatwaves due to climate
615   change and irrigation, *Nat Commun*, *9*, doi:ARTN 289410.1038/s41467-018-05252-y.

616   Kendy, E., J. X. Wang, D. J. Molden, C. Zheng, C. M. Liu, and T. S. Steenhuis (2007), Can urbanization
617   solve inter-sector water conflicts? Insight from a case study in Hebei Province, North China Plain,
618   *Water Policy*, *9*, 75-93, doi:10.2166/wp.2007.046.

619   Keune, J., F. Gasper, K. Goergen, A. Hense, P. Shrestha, M. Sulis, and S. Kollet (2016), Studying the
620   influence of groundwater representations on land surface-atmosphere feedbacks during the European
621   heat wave in 2003, *J Geophys Res-Atmos*, *121*(22), 13301-13325, doi:10.1002/2016jd025426.

622   Kobayashi, S., et al. (2015), The JRA-55 Reanalysis: General Specifications and Basic Characteristics, *J*

Meteorol Soc Jpn, *93*(1), 5-48, doi:10.2151/jmsj.2015-001.

Kollet, S. J., I. Cvijanovic, D. Schuttemeyer, R. M. Maxwell, A. F. Moene, and P. Bayer (2009), The Influence of Rain Sensible Heat and Subsurface Energy Transport on the Energy Balance at the Land Surface, *Vadose Zone J*, *8*(4), 846-857, doi:10.2136/vzj2009.0005.

Kollet, S. J., and R. M. Maxwell (2006), Integrated surface-groundwater flow modeling: A free-surface overland flow boundary condition in a parallel groundwater flow model, *Adv Water Resour*, *29*(7), 945-958.

Kollet, S. J., and R. M. Maxwell (2008), Capturing the influence of groundwater dynamics on land surface processes using an integrated, distributed watershed model, *Water Resour Res*, *44*(2), doi:Artn W0240210.1029/2007wr006004.

Leng, G., L. R. Leung, and M. Huang (2017), Significant impacts of irrigation water sources and methods on modeling irrigation effects in the ACME Land Model, *J Adv Model Earth Sy*, *9*(3), 1665-1683, doi:10.1002/2016MS000885.

Li, L. (2013), Development of a Numerical Model of Regional Groundwater Flow and its Application to the North China Plain, 97 pp, China University of Geosciences (Beijing), Beijing.

Liu, C. M., J. J. Yu, and E. Kendy (2001), Groundwater exploitation and its impact on the environment in the North China Plain, *Water Int*, *26*(2), 265-272.

Liu, J., C. Zheng, L. Zheng, and Y. Lei (2008), Ground water sustainability: Methodology and application to the North China Plain, *Ground Water*, *46*(6), 897-909.

Lloyd, J., and J. A. Taylor (1994), On the Temperature-Dependence of Soil Respiration, *Funct Ecol*, *8*(3), 315-323, doi:Doi 10.2307/2389824.

Maxwell, R. M., F. K. Chow, and S. J. Kollet (2007), The groundwater–land-surface–atmosphere connection: Soil moisture effects on the atmospheric boundary layer in fully-coupled simulations, *Adv Water Resour*, *30*(12), 2447-2466, doi:https://doi.org/10.1016/j.advwatres.2007.05.018.

Maxwell, R. M., and L. E. Condon (2016), Connections between groundwater flow and transpiration partitioning, *Science*, *353*(6297), 377-380.

Maxwell, R. M., L. E. Condon, and S. J. Kollet (2015), A high-resolution simulation of groundwater and surface water over most of the continental US with the integrated hydrologic model ParFlow v3, *Geosci Model Dev*, *8*(3), 923-937, doi:10.5194/gmd-8-923-2015.

Maxwell, R. M., L. E. Condon, S. J. Kollet, K. Maher, R. Haggerty, and M. M. Forrester (2016), The imprint of climate and geology on the residence times of groundwater, *Geophys Res Lett*, *43*(2), 701-708, doi:10.1002/2015gl066916.

Maxwell, R. M., and S. J. Kollet (2008), Interdependence of groundwater dynamics and land-energy feedbacks under climate change, *Nat Geosci*, *1*(10), 665-669, doi:10.1038/ngeo315.

Maxwell, R. M., J. K. Lundquist, J. D. Mirocha, S. G. Smith, C. S. Woodward, and A. F. B. Tompson (2011), Development of a Coupled Groundwater-Atmosphere Model, *Mon Weather Rev*, *139*(1), 96-116, doi:10.1175/2010mwr3392.1.

Maxwell, R. M., and N. L. Miller (2005), Development of a coupled land surface and groundwater model, *J Hydrometeorol*, *6*(3), 233-247.

Pal, J. S., and E. A. B. Eltahir (2001), Pathways relating soil moisture conditions to future summer rainfall within a model of the land-atmosphere system, *J Climate*, *14*(6), 1227-1242, doi:Doi 10.1175/1520-0442(2001)014<1227:Prsmct>2.0.Co;2.

Pei, H. W., B. R. Scanlon, Y. J. Shen, R. C. Reedy, D. Long, and C. M. Liu (2015), Impacts of varying agricultural intensification on crop yield and groundwater resources: comparison of the North China Plain and US High Plains, *Environ Res Lett*, *10*(4), doi:Artn 04401310.1088/1748-9326/10/4/044013.

Pollack, H. N., J. E. Smerdon, and P. E. van Keken (2005), Variable seasonal coupling between air and ground temperatures: A simple representation in terms of subsurface thermal diffusivity, *Geophys Res Lett*, *32*(15).

Qin, H., G. Cao, M. Kristensen, J. C. Refsgaard, M. O. Rasmussen, X. He, J. Liu, Y. Shu, and C. Zheng (2013), Integrated hydrological modeling of the North China Plain and implications for sustainable water management, *Hydrol Earth Syst Sc*, *17*(10), 3759-3778.

674 Rabus, B., M. Eineder, A. Roth, and R. Bamler (2003), The shuttle radar topography mission - a new class
675   of digital elevation models acquired by spaceborne radar, *Isprs J Photogramm*, *57*(4), 241-262,
676   doi:10.1016/S0924-2716(02)00124-7.
677 Rahman, M., M. Sulis, and S. J. Kollet (2015), The subsurface-land surface-atmosphere connection under
678   convective conditions, *Adv Water Resour*, *83*, 240-249, doi:10.1016/j.advwatres.2015.06.003.
679 Scanlon, B. R., C. C. Faunt, L. Longuevergne, R. C. Reedy, W. M. Alley, V. L. McGuire, and P. B. McMahon
680   (2012), Groundwater depletion and sustainability of irrigation in the US High Plains and Central Valley,
681   *P Natl Acad Sci USA*, *109*(24), 9320-9325, doi:10.1073/pnas.1200311109.
682 Szilagyi, J., V. A. Zlotnik, and J. Jozsa (2013), Net Recharge vs. Depth to Groundwater Relationship in the
683   Platte River Valley of Nebraska, United States, *Groundwater*, *51*(6), 945-951, doi:10.1111/gwat.12007.
684 Taylor, R. G., et al. (2013), Ground water and climate change, *Nat Clim Change*, *3*(4), 322-329,
685   doi:10.1038/Nclimate1744.
686 Wang, S., J. Shao, X. Song, Y. Zhang, Z. Huo, and X. Zhou (2008), Application of MODFLOW and
687   geographic information system to groundwater flow simulation in North China Plain, China, *Environ.
688   Geol.*, *55*(7), 1449-1462.
689 Xue, L., W. Li, W. Yang, J. Li, and X. Zhu (2010), Numerical modelling on exploited shallow groundwater
690   flow in the plain of Haihe river basin [in Chinese with English abstract], *Geotech. Invest. Survey.*, *3*,
691   50-55.
692 Zeng, Y. J., Z. H. Xie, S. Liu, J. B. Xie, B. H. Jia, P. H. Qin, and J. Q. Gao (2018), Global Land Surface
693   Modeling Including Lateral Groundwater Flow, *J Adv Model Earth Sy*, *10*(8), 1882-1900,
694   doi:10.1029/2018ms001304.
695 Zhang, H., E. L. Wang, D. W. Zhou, Z. K. Luo, and Z. X. Zhang (2016), Rising soil temperature in China
696   and its potential ecological impact, *Sci Rep-Uk*, *6*, doi:ARTN 3553010.1038/srep35530.
697 Zhang, T., R. G. Barry, D. Gilichinsky, S. S. Bykhovets, V. A. Sorokovikov, and J. P. Ye (2001), An
698   amplified signal of climatic change in soil temperatures during the last century at Irkutsk, Russia,
699   *Climatic Change*, *49*(1-2), 41-76, doi:Doi 10.1023/A:1010790203146.
700 Zhang, X. (2007), Numerical simulation of the shallow groundwater in the Haihe Basin [in Chinese], *Haihe
701   Water Resour.*, *3*, 52-54.
702 Zhang, X., L. Xue, Q. Zhang, and J. Li (2008), Simulation of groundwater exploitation at early stage and
703   analysis on water budget in Haihe River Basin [in Chinese], *J. Arid Land Resour. Environ*, *9*, 102–107.
704 Zhang, Y. G., M. G. Schaap, and Y. Y. Zha (2018), A High-Resolution Global Map of Soil Hydraulic
705   Properties Produced by a Hierarchical Parameterization of a Physically Based Water Retention Model,
706   *Water Resour Res*, *54*(12), 9774-9790, doi:10.1029/2018wr023539.
707 Zou, J., Z. H. Xie, C. S. Zhan, P. H. Qin, Q. Sun, B. H. Jia, and J. Xia (2015), Effects of anthropogenic
708   groundwater exploitation on land surface processes: A case study of the Haihe River Basin, northern
709   China, *J Hydrol*, *524*, 625-641, doi:10.1016/j.jhydrol.2015.03.026.
710
711